Journal of Fluids and Structures (2002) **16**(8), 1145–1176
doi:10.1006/jfls.2002.0468 available online at http://www.idealibrary.com on IDEAL®

A SIMULATION OF THE TURBULENCE RESPONSE OF HEAT EXCHANGER TUBES IN LATTICE-BAR SUPPORTS

M. A. Hassan, D. S. Weaver and M. A. Dokainish

Department of Mechanical Engineering, McMaster University, 1280 Main street West Hamilton, Ont, Canada, L8S 4L7

(Received 16 November 2000; and in final form 7 January 2002)

Tube failures due to excessive flow-induced vibrations are a major concern with regards to the operation of heat exchangers in nuclear power and chemical process plants. Among the possible excitation mechanisms, turbulence-induced forces have a persistent effect and thus are an important factor in determining the long-term reliability of heat exchangers. Impact forces which occur when tube/support collisions take place play a vital role in determining tube wear. To address this issue, a tube/support interaction model was implemented in an in-house finite element program and validated against three published examples. Pseudo-forces in conjunction with modal superposition were utilized in solving the nonlinear equations of motion of loose tubes in lattice-bar supports. Time-domain simulations of the nonlinear response of the tube are presented to determine the effect of various tube and support parameters on the vibratory characteristics of the systems. Special attention was paid to the effect of increased clearance on the response of tubes in lattice-bar supports. The tube response, impact force and contact ratio were analysed and represented in dimensionless form. The dimensionless parameters developed proved effective in collapsing the data pertaining to different flow velocities over single curves. These are useful in identifying the roles of several key variables in altering tube dynamics. Moreover, these parameters may also be used to scale the results to account for differences in geometrical and material properties.

1. INTRODUCTION

Heat exchangers have historically been among the most troublesome components in nuclear power and chemical process plants. Problems arise mainly as a consequence of tube failure. While tube failure is often attributed to corrosion at the support locations, tube fretting wear due to flow-induced vibration has been recognized as a significant contributor. These destructive flow-induced vibrations are due to a number of different mechanisms, usually classified as fluid-elastic instability, vortex shedding and turbulence buffeting (Blevins 1979; Pettigrew 1981; Païdoussis 1982; Weaver & Fitzpatrick 1988). Fluid-elastic instability is characterized by the development of large amplitude self-excited oscillations when the flow velocity exceeds a critical value. Through this mechanism, tubes may fail in a short period of time. In an attempt to avoid such destructive vibrations, design restrictions are imposed, which include reducing the flow velocity or increasing the tube natural frequencies. The latter is usually accomplished by installing tube supports at a number of locations to provide a stiffer configuration. Tube/support assemblies are usually loose-fitting due to manufacturing considerations which require these clearances to

0889-9746/02/081145 + 32 $35.00/0

facilitate tube bundle assembly and to accommodate thermal expansion. The number and locations of these supports are chosen so that stability prevails at the maximum design flow rates. However, other sources of excitation, such as turbulence, are omnipresent and cannot be avoided. Turbulence provides enough energy to induce significant vibrations of tubes inside the support space. When tube response due to turbulence exceeds the clearance in the tube support, initially centred tubes will strike the supports. Alternatively, a similar effect will be produced when tubes, initially in contact with the supports, are temporarily excited off the support by turbulence forces. These collisions result in impact and sliding forces at the tube/support interface. This environment provides favourable conditions for tube wall thinning, and in some cases, through-wall wear and tube failure (Païdoussis 1982). Typically, tube failure results in unplanned outages and very expensive downtime, particularly in nuclear power plants. Through fretting wear, turbulence-induced random vibrations may determine the long-term reliability of tube bundles and hence the heat exchangers. Therefore, estimating turbulence-induced response is an important step towards successfully evaluating the damage due to fretting wear and extending the life of heat exchangers.

The problem of loosely supported tube dynamics has captured the interest of numerous researchers, resulting in an increased volume of research and investigative work on this subject in the past three decades. Many experimental investigations have been conducted to study the nonlinear tube response and to characterize tube wear [see, for example, Weaver & Schneider (1983), Chen *et al*. (1985), Haslinger *et al*. (1987), Antunes *et al*. (1990b), Taylor *et al*. (1995)]. Additionally, numerical investigations utilizing the finite element method have been conducted to simulate the nonlinear tube response. Some of these studies considered tubes supported by loose baffle plates (Rogers & Pick 1977; Sauvé & Teper 1987; Rao *et al*. 1987), broached–hole (Fisher *et al*. 1991), and flat-bar supports (Yetisir & Weaver 1986). Some of these studies reported good correlation to experimental results.

Various support geometries currently used by manufacturers in heat exchanger U-bends were discussed by Weaver & Schneider (1983). The geometry of the support affects the dynamics of the tube due to variances in the contact configurations. Drilled and broached-hole support plates were used in many early heat exchanger designs. Other support arrangements, such as lattice-bar and flat-bar supports, are often utilized in the straight leg and U-bend regions in the newer steam generator designs. However, there is virtually no reference in the open literature regarding the effect of these particular support configurations on the vibratory behaviour of the tubes.

Lattice-bar supports have a relatively complex contact configuration due to the number of possible tube/support contact points. Moreover, lattice support geometry, when combined with tube-to-support clearance, offset and misalignment, yields a highly complex problem. Apart from the obvious interest in enhancing and refining the computational methods used for tube response prediction, it is also necessary to progress in the understanding and characterization of the support signature on tube behaviour. The understanding of tube dynamics in the presence of these types of loose supports and the associated fretting wear are still rather limited.

The aforementioned investigations produced abundant numerical and experimental data that need further interpretation. In addition, a shortcoming of the present body of analysis is due to its treatment of specific configurations and flows. This makes it difficult to apply the results to situations involving different flows or tube/support configurations. In an effort to further the understanding of the fundamental mechanism of tube/support interaction, this paper presents a numerical investigation of loosely supported tube dynamics. A more general approach has been initiated in an attempt to derive scaling

parameters that reduce the nonlinear random tube response to a dimensionless form convenient for providing physical insights and for design purposes. The computer code developed is evaluated against published results and then used to predict turbulence-excited tube response in various lattice-bar support arrangements.

2. NONLINEAR TUBE RESPONSE CALCULATIONS: INDAP CODE

2.1. Formulation of Tube Dynamics

Within the finite element framework, the equation of motion of a tube is written as

$$[M]\{\ddot{u}\} + [C]\{\dot{u}\} + [K]\{u\} = \{F_e(t)\}, \tag{1}$$

where $\{\ddot{u}\}, \{\dot{u}\}$ and $\{u\}$ represent the vector of displacement and its temporal derivatives; $[M], [C]$ and $[K]$ are the mass, the damping and the stiffness matrices, respectively, while $\{F_e(t)\}$ is the external fluid excitation (turbulence, fluid-elastic, etc.). Tube-to-support contact takes place when the normal component of tube displacement and/or misalignment at the support location exceeds the support gap. Contact is generally treated by introducing a displacement-dependent stiffness component to the system equations of motion. The standard finite element procedures for global contact of solids can be used to solve for the system response. However, these procedures often require extensive computation and contact searching algorithms which are costly. A substantial saving in the computational cost can be obtained by using the pseudo-force approach for problems in which the nonlinearities are localized (Dokainish & Subbaraj 1989). Tubes with loose supports are a typical example of this type of nonlinearity. In this method, it is sufficient to describe tube motion with the familiar beam equation, while these nonlinearities due to tube/support contact can be represented by external forces:

$$[M]\{\ddot{u}\} + [C]\{\dot{u}\} + [K]\{u\} = \{F_e(t)\} + \{F_i(u, \dot{u}, t)\}, \tag{2}$$

where $\{F_i(u, \dot{u}, t)\}$ is the pseudo-force vector containing the impact forces and is given by

$$\{F_i(u, \dot{u}, t)\} = [C_{NL}]\{\dot{u}\} + [K_{NL}]\{u\}, \tag{3}$$

in which C_{NL} and K_{NL} are the nonlinear contributions of the contact to the damping and stiffness matrices, respectively. Impact forces are computed by considering a spring and a damper added at the support location (Figure 1). If the normal component of a tube's displacement $u_n(t)$, exceeds the radial support clearance, C_r, contact occurs. The normal component of the impact force is computed as follows:

$$F_{\text{imp}} = F_{\text{spr}} + F_{\text{dmp}}, \tag{4}$$

where F_{spr} and F_{dmp} are the spring and damping force defined as (Sauvé & Teper 1987)

$$\begin{aligned} F_{\text{spr}} &= K_{\text{spr}}(|u_{\text{n}}(t)| - C_{\text{r}}), \\ F_{\text{dmp}} &= C_{NL}\dot{u}_n(t) \\ &= 1{\cdot}5\beta K_{\text{spr}}(|u_n(t)| - C_{\text{r}})\dot{u}_n(t), \end{aligned} \tag{5}$$

in which K_{spr} and β are the spring stiffness and the material damping coefficient, respectively.

In addition to the normal contact force, friction forces act in a direction parallel to the support surface and oppose the relative motion of the tube. The proper modelling of these forces is a difficult problem. If a tube is preloaded against its support, the sliding velocity will be zero until the fluid loading is sufficient to overcome the "sticking" frictional force.

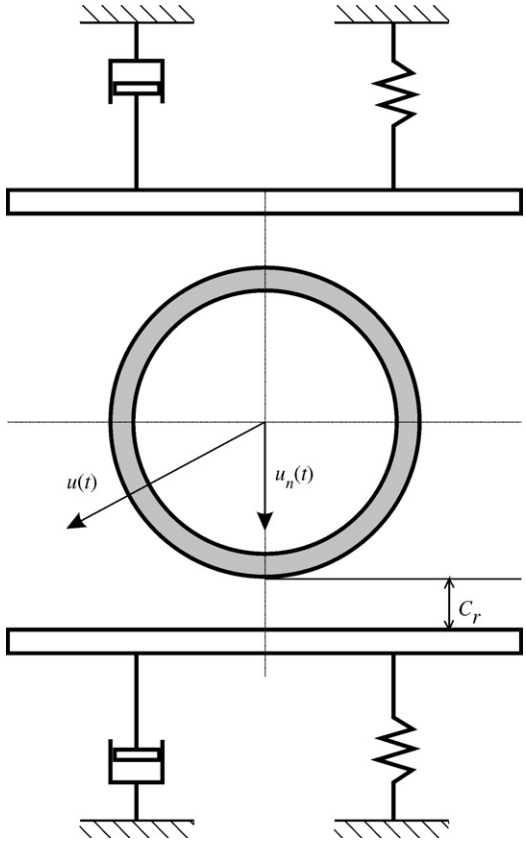

Figure 1. Spring–damper model for a flat-bar support.

This ''sticking'' friction is usually significantly higher than that associated with sliding. Obtaining good experimental data for these forces is difficult and the highly nonlinear ''stick–slip'' behaviour often leads to numerical instabilities in mathematical modelling. Antunes *et al.* (1990a) gave an excellent account of these difficulties and proposed a heuristic model with adherence stiffness and damping terms. When preloads up to 50N and high coefficients of friction were used in their computations, they found that neglecting the frictional effect caused significant overestimation of wear. However, their wear predictions were less sensitive to frictional forces when no preload was present. Tan & Rogers (1996) designated the Antunes *et al.* (1990a) model as a ''spring–damper friction model'' (SDFM) and found that it led to numerical difficulties when applied to sliding on a surface. In attempting to use the SDFM in the development of the present code, similar problems were encountered. As a result, Tan & Rogers (1996) introduced a ''force-balance friction model'' (FBFM) which they claimed could capture the stick–slip motion without numerical instabilities. In comparing their FBFM prediction with the experimental data, they found that it overestimated the wear work rate at preloads above 3N but underestimated the wear work rate by about 40% for no preload. They suggested that the difference may be due to the experimental error. What has emerged from these works is the importance of modelling stick–slip behaviour in the presence of significant preloading of the tube against the support. More research is necessary, however, to improve the agreement between experiments and theory.

In the present research, the tube is assumed to be centred in its supports with no initial contact. Under these conditions, a typical tube/support contact duration is less than 10 ms and, as indicated by Antunes *et al.* (1990a), the work rate is not expected to be sensitive to the friction model used. Indeed, this was found by Rao *et al.* (1987) for a case of no preload. Thus, a simple "velocity-limited friction model" (VLFM) as used by Rogers & Pick (1977), Fisher *et al.* (1991) and Yetisir & Weaver (1986) was employed in the present study. Since sticking, which tends to prevent wear, is not addressed in this model, the results are expected to yield conservative work rate estimates. A more sophisticated model would be required if an initial contact or a significant preload were considered.

In the classical friction model, also called Coulomb's friction model, the frictional force F_f, between two bodies subjected to a normal load, F_N, is given by

$$F_f < \mu_s F_N \quad \text{if} \quad V_t = 0, \tag{6a}$$

$$F_f = -\text{sign}(V_t)\mu_d F_N \quad \text{if} \quad V_t \neq 0, \tag{6b}$$

where V_t is the tangential velocity of the tube relative to the support, and μ_s and μ_d are the static and the dynamic coefficients of friction, respectively. Equations (6a) and (6b) represent the static and dynamic friction conditions, respectively. Numerical problems arise when using equation (6a) because of the rapid change in the friction force as the tangential velocity changes signs. A remedy for this problem can be found in the VLFM. This model uses a combination of the Coulomb and the viscous friction models. A limiting velocity V_o is defined such that within the interval $|V_t| \leqslant V_o$ the friction force is proportional to the tangential velocity V_t as follows.

$$F_f = -\left(\frac{V_t}{V_o}\right)\mu_s F_N \quad \text{if} \quad |V_t| \leqslant V_o. \tag{7}$$

Equation (6b) can be used if $|V_t| > V_o$. Using the VLFM improves the numerical stability of the solution. Moreover, the classical friction model can be obtained as a special case by setting this limiting velocity to zero. The VLFM was used in investigating tube/support contact in previous investigations and was found to give a reasonable tube response prediction (Rogers & Pick 1977; Yetisir & Weaver 1986; Fisher *et al.* 1991).

Using the pseudo-force method, the normal and shear forces described above are introduced to the system as external forces. If the force time history is known, the displacement at the end of the time step can be calculated. However, this is not the case when impact occurs, because the force at the end of the time step depends on the tube response, and is therefore unknown. Accordingly, an iterative procedure is used to calculate the time history of the displacement and the impact forces.

Davis & Rogers (1979) showed analytically that the motion of a tube can be described as a linear combination of the unconstrained modes. This permits for the use of modal superposition to solve for the system response, thereby saving a considerable computational effort. The response converges rapidly to the correct solution as the number of modes used in the analysis increases. Typically, less than 10–20 modes in each direction are sufficient to achieve a reasonable representation of the constrained tube motion and the contact forces (Antunes *et al.* 1990a).

In this procedure, support nodes are monitored to detect any overlaps, i.e., displacements exceeding the support gap. If an overlap is detected, the displacement vector is used to calculate the contact forces that will remove this overlap. These forces are then applied as external forces to the system and a new force vector is obtained. This process is repeated until the nonlinear forces converge. The modelling of impact forces is strongly dependent on the contact configuration dictated by the support geometry. This

tube/support interaction model was incorporated in incremental nonlinear dynamic analysis program, (INDAP) which is an in-house finite element program (Dokainish 1988).

3. VERIFICATION CASES

3.1. Single-Span Tube

A comparison with a documented case (Yetisir 1985) was made to examine the validity of the implemented algorithm in predicting the displacement and impact force time histories. The model utilizes a cantilever tube with a loose support at the free end. The tube is 1 m long, with a 15·88 mm outer diameter, and a 10·03 mm inner diameter. The elastic modulus and the mass density are 230 GPa and 7920 kg/m^3, respectively. The tube was modelled using 20 12-dof (degrees of freedom) beam elements. A sinusoidal concentrated force is applied at the tip of the tube. Thirty-two modes, each with 1% critical damping, were used in the analysis. The displacement and force time histories of the documented case (Yetisir 1985) and INDAP are shown in Figure 2. The comparison indicates quite a reasonable agreement in the displacement trace as well as in the impact force and duration.

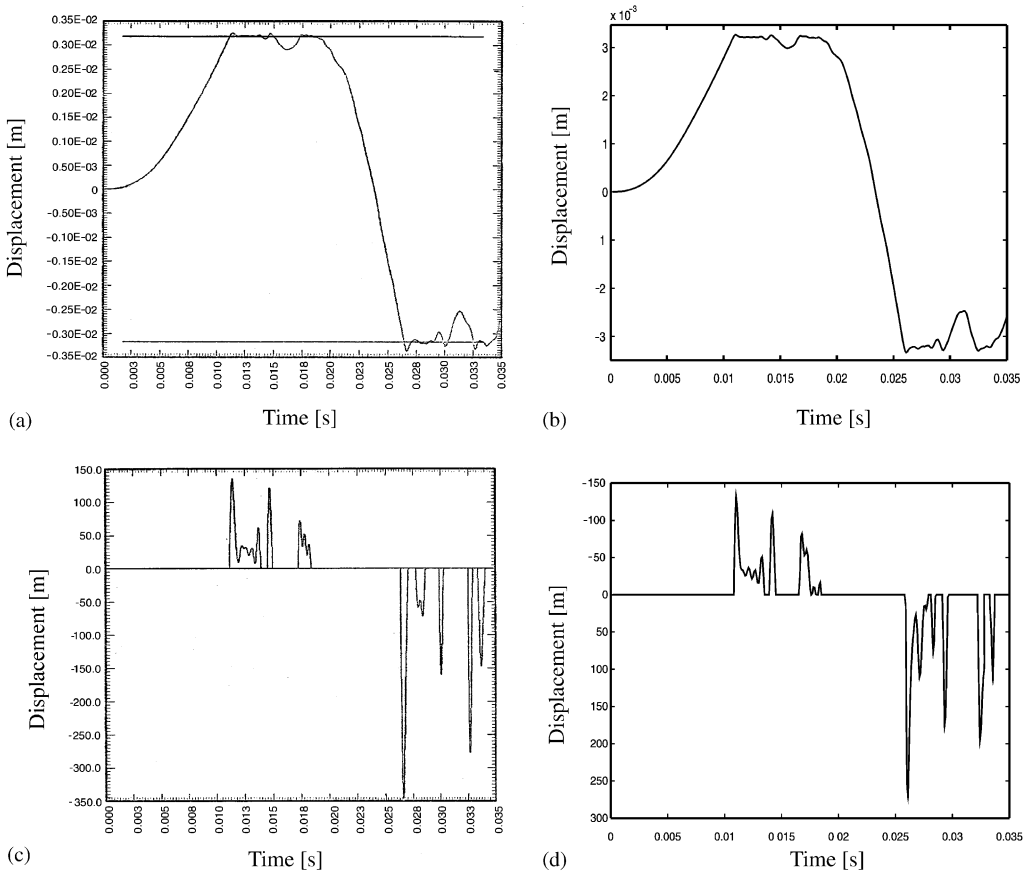

Figure 2. Displacement and impact force traces for a single–span tube: (a), (c) Yetisir (1985); (b), (d) current work.

3.2. Multi-Span Tube

Sauvé & Teper (1987) developed a direct implicit (Newmark) integration code H3DMAP (Hydro 3 Dimensional Matrix Analysis Program) to simulate the nonlinear dynamic impact response of multi-supported tubes. Later, Sauvé (1996) modified the H3DMAP code utilizing an explicit (central difference) integration scheme. Sauvé & Teper (1987) presented simulation results for a four–span model of a typical process equipment arrangement subjected to high flow forces (Figure 3). The flow excitation was modelled as a distributed force with alternating directions over each span.

The time history of the response was obtained for a number of clearances for 10 driving cycles (0–0·25 s). Time history traces of both the displacement and the impact force were obtained using INDAP and compared to the published traces (Figure 4). The comparison of the time history traces by INDAP and by H3DMAP (Sauvé & Teper 1987) shows reasonable agreement. The r.m.s. impact forces at all supports were obtained over 5–10 driving cycles. The same example was used by Fisher *et al*. (1989) to verify the VIBIC (VIbration of Beams with Intermittent Contact) code which utilized an explicit time integration of the modal equations of motion. Figure 5 shows the predicted r.m.s. impact force at each support for four different radial clearances along with a comparison of the predictions by H3DMAP and VIBIC. The predicted r.m.s. impact forces obtained by INDAP agree reasonably well with those of H3DMAP and VIBIC, there being no systematic differences among the predictions of the three codes. The differences in the displacement and impact force time histories as well as the predicted values of the r.m.s. force may be attributed to several reasons. Firstly, the number of modes included in the analysis may slightly affect the predicted impact force. While H3DMAP utilizes the direct integration approach in which the number of modes included is limited by the number of degrees of freedom and the size of the elements, VIBIC and INDAP utilize the modal superposition approach in which a finite number of modes are considered. Secondly, H3DMAP utilizes a variable time step size algorithm to accelerate the rate of the convergence of the nonlinear solution. On the other hand, the choice of the time step in INDAP is based on the accuracy required by the highest participating mode. These differences in the time step can affect the details of the impact force. Finally, it should be

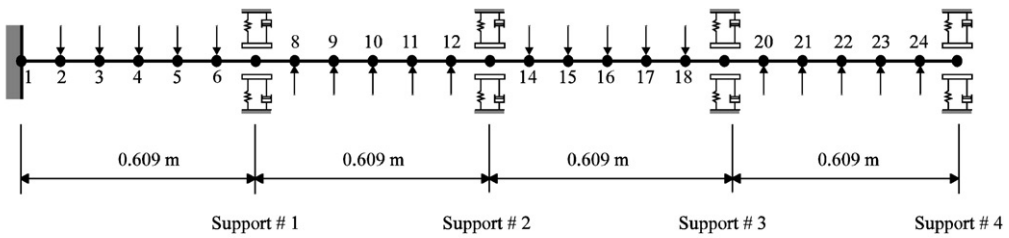

Tube : 2.436 m Long, 15.9 mm OD, 13.6 mm ID
Material : $E=2.07\times10^{11}$ Pa, $\tilde{n}=7.87\times10^{3}$ kg/m^3

Support : $K_{gap} = 1.75\times10^{7}$ N/m, $C_{gap} = 0.28$ N.s/m
Damping : $C=\hat{a}M+\tilde{a}K$, $\hat{a}=0.1526$, $\tilde{a}=1.7983\times10^{-5}$

Forcing Function : $F_i = 4.2 \sin(2\pi f t)$ i = 2-6, 14-18
$F_i = -4.2 \sin(2\pi f t)$ i = 8-12, 20-24
$F_{25} = 2.1 \sin(2\pi f t)$ f = 40 Hz

Figure 3. Four-span tube subjected to high flow forces (Sauvé & Teper 1987).

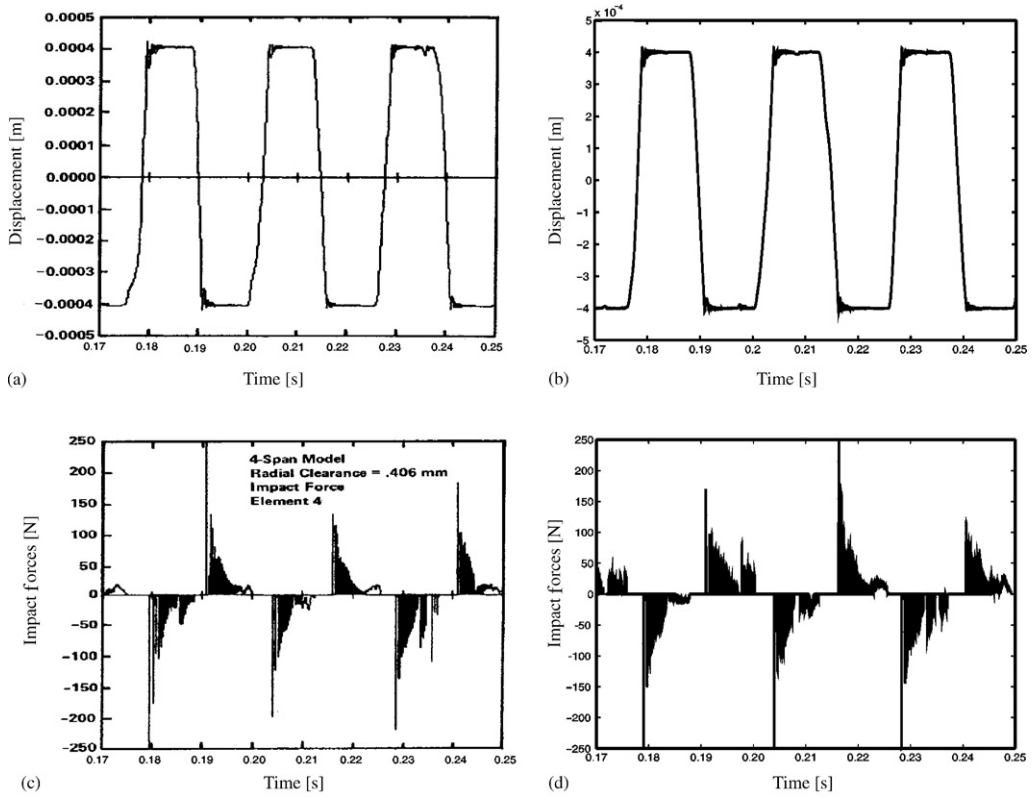

Figure 4. Displacement and impact force traces at support No. 4 for a multi–span tube: (a), (c) Sauvé & Teper (1987); (b), (d) current work.

noted that an exact replica of the displacement and impact force time histories may not be achieved. This is due to the sensitivity of the solution of the nonlinear system to the integration scheme as well as small differences in the solution parameters such as time step size, damping, etc. However, the purpose of the nonlinear analysis of the heat exchanger tubes is not to investigate the details of individual impacts but to assess the parameters that affect the mean properties of tube/support interaction. Therefore, if tube/support interaction parameters are averaged over a sufficiently long period, a better agreement would result.

4. SINGLE-SPAN TUBE SUBJECTED TO TURBULENCE

4.1. Finite Element Model

To investigate the effect of lattice-bar supports and clearances, a single-span tube 2 m long, fixed at one end and loosely supported at the free end, is considered [Figure 6(a)]. The outer tube diameter is 0·015 m with a wall thickness of 0·0015 m. The tube mass per unit length and Young's modulus are 0·7397 kg/m and 230 GPa, respectively. The tube is loosely supported by a lattice–bar support which consists of two pairs of bars arranged to form a 60° diamond-shaped support clearance [Figure 6(b)]. Lattice-bar supports can be categorized according to the support offset (e) and the angle between adjacent supports (α)

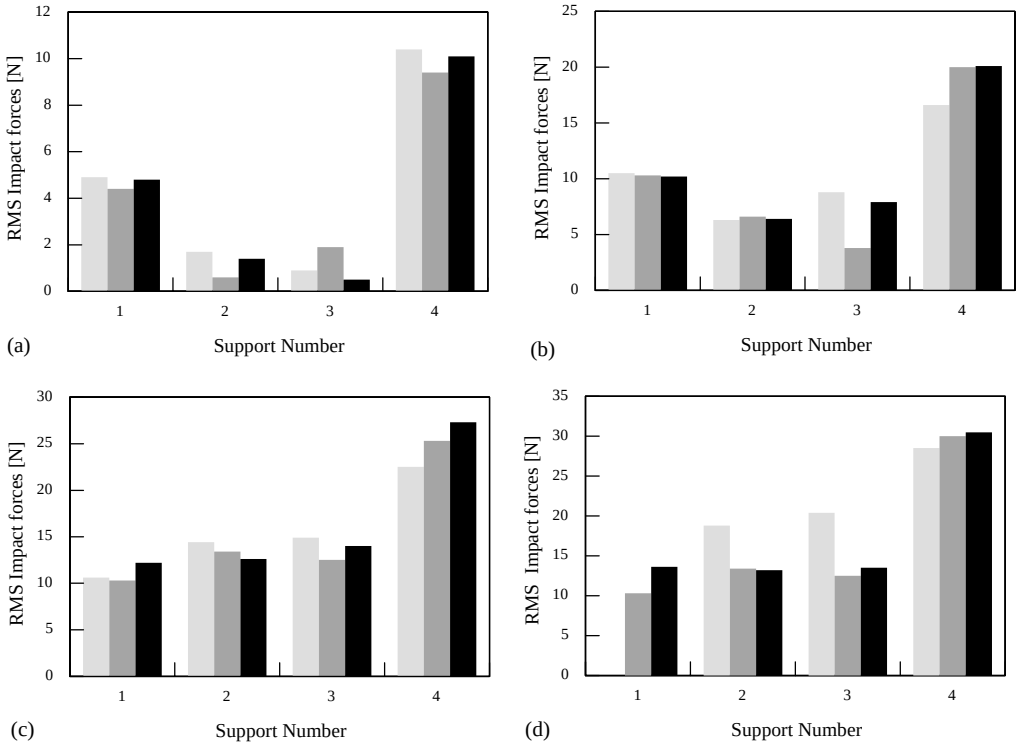

Figure 5. The r.m.s. impact force for different radial clearances: (a) 0·001 mm; (b) 0·2 mm; (c) 0·406 mm; (d) 0·6 mm. Computations by □ VIBIC; ▨ H3DMAP; ■ INDAP.

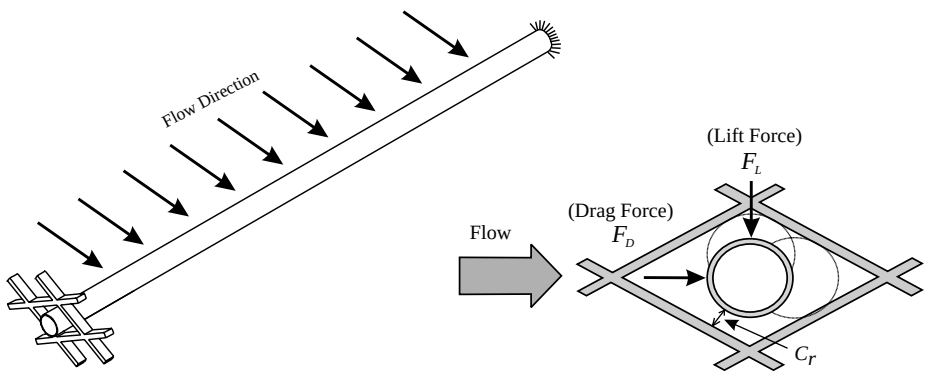

Figure 6. Single-span tube with a lattice-bar support.

as shown in Figure 7, where d is the tube diameter and C_r is the radial clearance of a centred tube. In the case of a lattice-bar support for a triangular tube array, the angle α is 120°. Tubes are discretized into 20 12-dof beam elements.

The loose support is located at the free end ($x/L = 1{\cdot}0$). An approximate range of 10^5–10^7 N/m for the support stiffness has been reported in the literature (Rogers & Pick 1977; Axisa *et al.* 1988; Fricker 1992). However, these papers demonstrated that the impact forces are rather insensitive to the support stiffness in this range. Thus, an intermediate

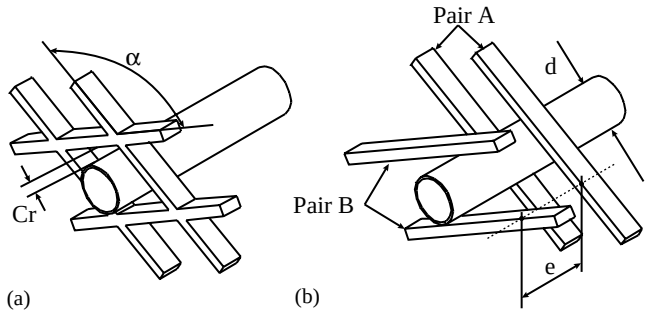

Figure 7. Lattice-bar supports: (a) without offset; (b) with offset.

support stiffness of 10^6 N/m was used in the present analysis. The value of the support damping coefficient (β) used in this work was 0·25 s/m for steel (Hunt & Crossley 1975). With respect to the coefficient of friction, a range of 0·0–0·5 has been reported in the literature (Fisher *et al*. 1991; Rao *et al*. 1997). Haslinger & Steininger (1995) recommended values of 0·36–0·40 for flat-bar supports. In this analysis, a single coefficient of friction value of 0·1 was utilized since this value represents a reasonable lower bound.

4.2. Turbulence Excitation Modelling

Random turbulence excitation is a significant vibration mechanism of tubes subjected to crossflow. For the inlet region of heat exchangers, the upstream tubes are excited by the turbulence generated upstream of the inlet nozzle or within the inlet port, baffles, etc. Such excitation is governed by the upstream components and may be referred to as far-field excitation. The interior tubes are excited by the turbulence generated within the bundle. This in turn is governed by the tube bundle geometry. In general, fluid excitation due to turbulence is modelled as randomly distributed forces. The bounding power spectral density (PSD) measured by Oengören & Ziada (1995) for a tube array of pitch-to-diameter ratio (P/D) of 1·61 was utilized in this work to generate the time-domain fluid forces. However, the results are independent of the choice of bounding spectra when presented in the dimensionless form developed in this study.

To implement this approach, the empirically based PSD curve of turbulence excitation is obtained depending on the flow velocity, the tube's diameter and array geometry. This PSD curve is then transformed into a force–time record using an inverse Fourier transform algorithm with random phases. The resulting fluctuating forces are Gaussian in nature with a zero mean value. Two different force versus time records were used representing the fluid excitation in the lift and the drag directions. The lift force record contains only a fluctuating force component with a zero mean. On the other hand, the drag force record consists of the fluctuating force component superimposed on a static component representing the steady drag forces. These are then input into the nonlinear tube/support model [Equation (2)]. The fluid forces were applied at the beam elements nodes and computations were carried out for three levels of air-flow velocity, 4, 6, and 8 m/s.

4.3. Results and Discussion

For each support case study, 20 s of response time history were computed. The tube/support interaction parameters were averaged over the simulation time record excluding

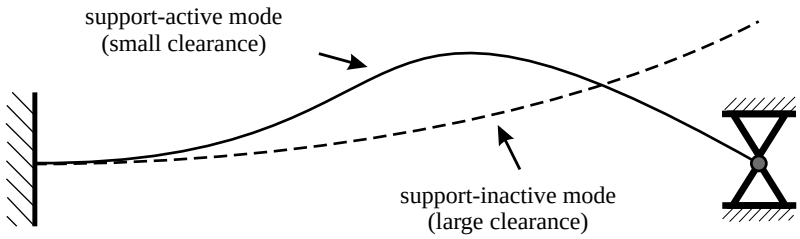

Figure 8. Support-active and -inactive modes for lattice-bar supports (response normal to the surface of supports).

the initial transient period. The power spectral density (PSD) of the tube response (at the first unconstrained node away from the fixed end) was obtained. A wide range of radial clearance values ranging from 0·001 to 1 mm was examined. Because of the clearance, the tube can respond in different modes depending on the effectiveness of the support which can be categorized as either support-active or support-inactive modes (Chen *et al*. 1985). For the support-active mode, the tube boundary conditions are considered as fixed–hinged. On the other hand, the support-inactive mode corresponds to fixed–free end conditions. These two modes are shown in Figure 8. The presence of either of these modes is dependent on the clearance/excitation level combination. It should be noted that the presence of pure support-active or support-inactive modes represents extreme conditions in which the tube response will be linear. At intermediate conditions, the response is expected to be strongly nonlinear.

4.3.1. Response spectra

Figure 9 shows samples of the response PSD of a tube with a lattice-bar support and a zero–support offset, calculated at the first unconstrained node away from the fixed end. The spectra presented are for tubes with different clearances which are subjected to the same flow velocity (4 m/s). Depending on the clearance value, two groups of frequency peaks can be easily identified. For a small clearance [Figure 9(a)], the PSD of the tube response is dominated by frequencies corresponding to the natural frequencies of the fixed–hinged configuration (support-active). At large clearances, the PSD of the tube response is dominated by the lower frequency free modes of the tubes (support-inactive) as shown in Figure 9(c). Figure 9(b) depicts the PSD of the tube response for an intermediate clearance where a transition between the modes takes place. This behaviour is known as the mode switch and was also observed by Chen *et al*. (1985). Note that the intermediate response spectrum appears noisy with rather poorly defined natural frequencies.

4.3.2. Contact ratio

The contact ratio is defined as the summation of the time intervals during which tube/support contact is maintained divided by the total duration of the time record. The total duration of the time record was chosen to be sufficiently large that the results were independent of the time record. This was different for each case treated and determined by successive numerical trials.

In keeping with one of the purposes of this study, to present general results in terms of dimensionless parameters, the flow velocity parameter used will be reduced velocity, U_R, specified as

$$U_R = \frac{V_f}{fd}, \tag{8}$$

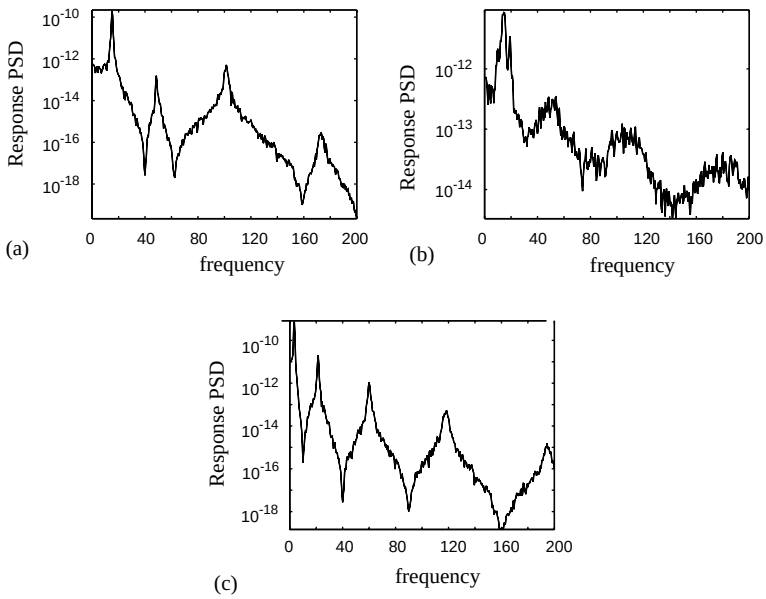

Figure 9. Response spectra of the tube with lattice-bar support (0% offset) and varying clearance: (a) 0·001 mm; (b) 0·3 mm; (c) 0·7 mm.

where V_f,f and d are the flow velocity, the tube fundamental frequency and the tube diameter, respectively. Figure 10(a) shows the contact ratio (C_t) of a tube in a lattice–bar support for various reduced velocities. Above a clearance of about 0·1 mm, increasing the reduced velocity increases the contact ratio. For a given reduced velocity, the contact ratio remains approximately constant for a range of clearances (C_r). This is because the tube is kept in continuous contact with the support by the steady drag component. A further increase in the clearance beyond this range results in a sharp decrease in the contact ratio. It then levels off asymptotically to zero. This behaviour is observed for all three reduced velocities examined. The mode switch takes place in the clearance range where a sharp drop in the contact ratio occurs.

It is also observed that tubes with a similar excitation-to-clearance ratio have a similar vibration pattern. This is consistent with the findings of Yetisir & Weaver (1986), who concluded that doubling the clearance produces results similar to that of halving the excitation level. Low excitation leads to a low tube vibration amplitude. The tube can, therefore, vibrate within the support space without contact, provided the clearance is sufficiently large. Now, if a higher excitation is applied to a tube with the same clearance, the tube would contact the support because it is able to freely deflect more than the support clearance allows. The higher the excitation, the higher the tube deflection which in turn leads to a higher contact ratio.

It follows that the response of the free tube could be a suitable parameter to normalize the clearance. To illustrate this idea, the contact ratio was plotted as a function of the dimensionless clearance [Figure 10(b)]. The dimensionless clearance was obtained by dividing the radial clearance (C_r) by the r.m.s. support–inactive resultant response (d_{rsi}), i.e., the linear response of a tube at the support location without an end support. Using this dimensionless parameter (C_r/d_{rsi}) leads to a significant data collapse of the contact ratio for various reduced velocities [Figure 10(b)]. Moreover, it is found that the mode

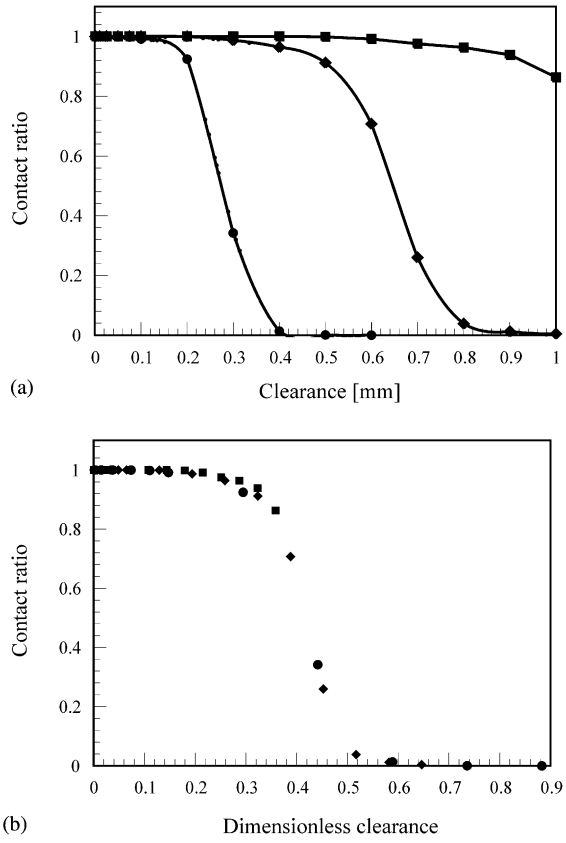

Figure 10. Effect of the clearance on the contact ratio for configuration 1 (no offset): ●, $U_R = 77{\cdot}8$; ◆ $U_R = 116{\cdot}7$; ■ $U_R = 155{\cdot}5$: (a) clearance, mm; (b) dimensionless clearance.

switch observed in the response spectra takes place in the same dimensionless clearance range ($0{\cdot}4 < C_r/d_{rsi} < 0{\cdot}5$) for all reduced velocities.

4.3.3. *Impact forces*

The r.m.s. impact force utilized here is the standard definition which is computed as follows:

$$(F_{\text{imp}})_{\text{rms}} = \left(\lim_{\text{T}\to\infty} \frac{1}{T} \int_0^T (F_{\text{imp}}(t))^2 \, \text{d}t \right)^{1/2}, \tag{9}$$

where $F_{\text{imp}}(t)$ and T are the instantaneous normal component of the impact force and the total time record length, respectively. For simplicity, the subscript "rms" will be dropped and F_{imp} will be used to express the r.m.s. impact force. The r.m.s. impact force (F_{imp}) depends on both the amplitude of the impact peaks and the contact duration. The higher the contact duration, the higher the impact forces will be (for identically centred tubes with identical loading conditions). Increasing the radial clearance decreases the contact ratio, which in turn decreases the r.m.s. impact force. In addition, inducing higher kinetic energy due to a higher reduced velocity results in higher impact forces. This is illustrated in Figure 11(a) which depicts the r.m.s. impact force values versus the clearance for various reduced

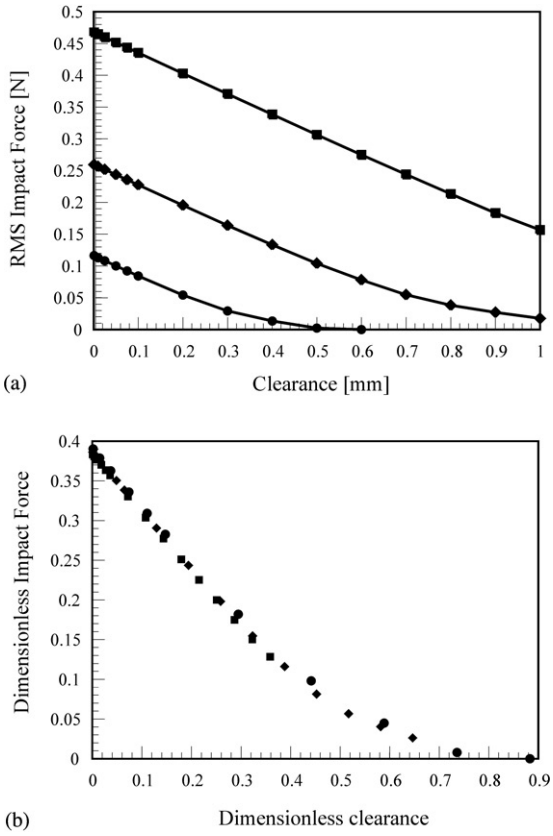

Figure 11. Effect of the clearance on the r.m.s. impact force for configuration 1 (no offset): ●, $U_R = 77{\cdot}8$; ◆ $U_R = 116{\cdot}7$; ■ , $U_R = 155{\cdot}5$. (a) R.m.s. impact force, N; (b) dimensionless r.m.s. impact force.

velocities. R.m.s. impact forces decrease linearly as the support clearance increases, then level off asymptotically to zero. For any clearance size, increasing the reduced velocity increases the r.m.s. impact force. Since the resulting impact force must be related to the level of excitation, it is logical to use the r.m.s. excitation forces to normalize the r.m.s. resulting impact force. The dimensionless r.m.s. impact force, F, is presented as $F = F_{imp}/(P_{tur}L)$, where F_{imp}, P_{tur} and L are the r.m.s. impact force, the r.m.s. distributed turbulence force per unit length (computed as the square root of the sum of squares of the lift and drag components), and the tube length, respectively. The dimensionless clearance used is the same as that used in Section 4.3.2. Using these dimensionless parameters, the r.m.s. impact force collapsed to a single curve for the same support configuration, as shown in Figure 11(b). At a near-zero clearance, the dimensionless impact force is 0·39. It is interesting to note that this dimensionless impact force is close to the theoretical value (0·375) of the support force at the pinned end of a clamped–pinned beam with a uniform load. With larger dimensionless clearances, it decreases linearly and becomes asymptotic to zero as contact with the support ceases.

4.3.4. Tube displacement

In Figure 12(a), the r.m.s. mid-span tube response in the lift direction, d_y, obtained by averaging the output of the displacement–time record of the nonlinear simulations, is

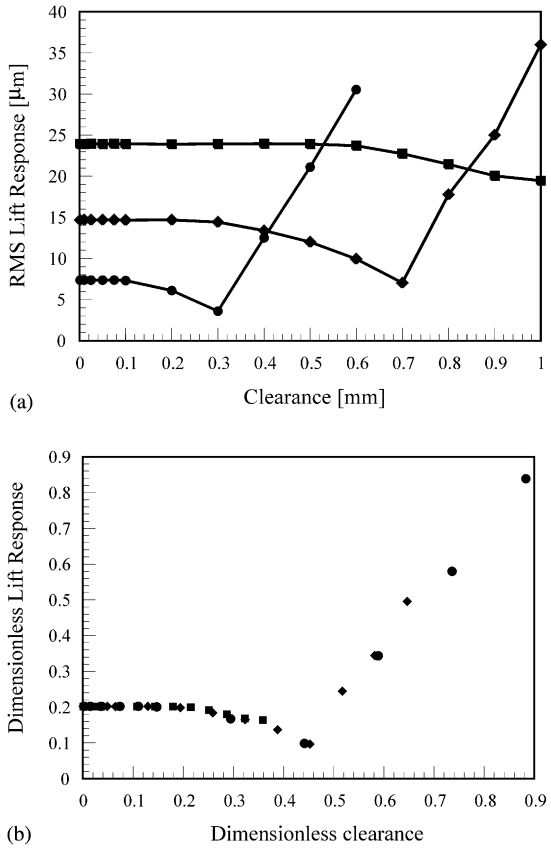

Figure 12. Effect of the clearance on the r.m.s. tube displacement in the lift direction for configuration 1 (no offset): ●, $U_R = 77{\cdot}8$; ◆, $U_R = 116{\cdot}7$; ■, $U_R = 155{\cdot}5$. (a) Mid-span tube displacement, μm; (b) dimensionless r.m.s. mid-span tube displacement.

plotted versus the radial clearance C_r, for various reduced velocities. The lift response shows a similar trend for all reduced velocities. At a very small radial clearance, the tube maintains continuous contact with the support. The lift response is approximately equal to that of a fixed–hinged configuration. As the radial clearance increases, intermittent contacts take place and higher modes are excited. This leads to a gradual decrease in the r.m.s. tube response. This gradual decrease of the tube response continues up to a certain clearance value where the mode switch occurs and the supports become less active. The tube response is then dominated by low frequency modes, and the r.m.s. tube response is almost proportional to the radial clearance. At larger support clearances, the r.m.s. response, as expected, approaches the support-inactive r.m.s. tube response. The point of minimum r.m.s. response, however, shifts to a larger clearance as the reduced velocity increases. The r.m.s. lift response and the support clearance are normalized by the r.m.s. lift support-inactive response and the resultant support-inactive response, respectively. Data for various reduced velocities are represented by a single curve using these dimensionless parameters [Figure 12(b)]. The dimensionless lift response for a near-zero clearance is approximately 0·2. This is the ratio of the constrained tube response (support-active) to the unconstrained tube response (support-inactive). At dimensionless clearances larger than 1·0, [not shown in Figure 12(b)], the dimensionless lift displacement

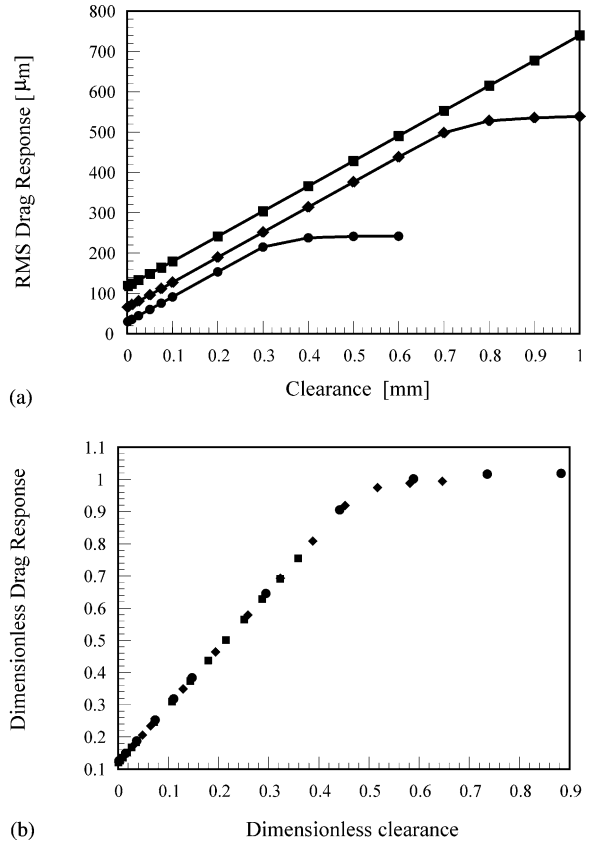

Figure 13. Effect of the clearance on the r.m.s. tube displacement in the drag direction for configuration 1 (no offset): ●, $U_R = 77{\cdot}8$; ◆, $U_R = 116{\cdot}7$; ■, $U_R = 155{\cdot}5$. (a) Mid-span tube displacement, μm; (b) dimensionless r.m.s. mid-span tube displacement.

approaches unity. The point of minimum dimensionless displacement for all reduced velocities is at a dimensionless clearance of 0·45.

Figure 13(a) shows the r.m.s. mid-span tube response (d_z) in the drag direction as a function of the support clearance for various reduced velocities. The effect of drag forces is evident where the tube drag response increases linearly as the clearance increases. This behaviour is maintained up to a certain clearance after which the response approaches the r.m.s. support-inactive tube response. By replacing both axes with dimensionless parameters, a single curve can be obtained, as shown in Figure 13(b). Again, the mode switch can be identified by the change of the slope at a dimensionless clearance of 0·45.

4.3.5. Work rate

Tube fretting wear is usually estimated by correlating the experimental wear with the computed work rate. Work rate (W_N) is calculated by averaging the product of the impact forces and the tube sliding displacement:

$$W_N = \frac{1}{T}\int_0^T F_N \, \mathrm{d}s, \tag{10}$$

where T, F_N, and $\mathrm{d}s$ are the averaging time, the normal impact force, and the sliding distance, respectively. Figure 14(a) shows the predicted work rate as a function of the

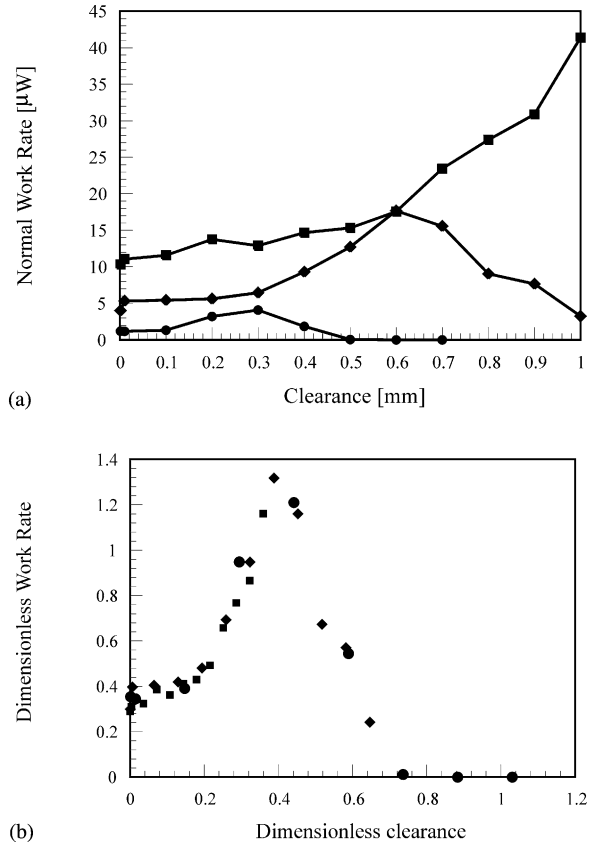

Figure 14. Effect of the clearance on the normal work rate for configuration 1 (no offset): ●, $U_R = 77{\cdot}8$; ◆, $U_R = 116{\cdot}7$; ■, $U_R = 155{\cdot}5$. (a) Normal work rate, μW; (b) dimensionless normal work rate.

clearance. The general behaviour of the work rate was the same for all reduced velocities under consideration. The normal work rate increases gradually as the clearance increases. The increase in the work rate continues to a certain clearance where less contact is being maintained and the mode switch takes place. A further increase in the clearance causes the work rate to drop dramatically. In reality, the work rate may continue to increase as the clearance increases because of the occurrence of fluid-elastic instability in the lowest unsupported mode. Fluid-elastic forces, however, are not considered in the present model. The values of the work rate were normalized by the input power due to turbulence. The total power absorbed by a tube of length L and mass per unit length m, was expressed by Yetisir *et al*. (1997) as

$$W_{\text{tur}} = \sum_{i=1}^{n} \frac{S_{FF}(f_i) J_i^2 L}{2m}, \tag{11}$$

where $S_{FF}(f_i)$ and J_i are the magnitude of the PSD of the local force per unit length and the joint acceptance for the ith mode, respectively. The work of Yetisir *et al*. (1997) utilized the input energy of the constrained system. However, in the present work, consistent with the rest of the dimensionless set, the input power is calculated based on the unconstrained modes. The clearance was also normalized by the r.m.s. support-inactive tube response.

TABLE 1
Summary of the dimensionless parameters

Parameter	Symbol	Dimensionless form
Radial clearance	C_r	C_r/d_{rsi}
R.m.s impact force	F_{imp}	$F_{\text{imp}}/(P_{\text{tur}}L)$
R.m.s lift response	D_y	d_y/d_{ysi}
R.m.s drag response	D_z	d_z/d_{zsi}
Normal work rate	W_N	W_N/W_{tur}

Notation

d_{rsi}	r.m.s. support-inactive resultant response.
P_{tur}	resultant r.m.s. turbulence force per unit length.
L	tube length.
d_{ysi}	r.m.s. support-inactive response in lift direction.
d_{zsi}	r.m.s. support-inactive response in drag direction.
W_{tur}	input power due to turbulence.

These dimensionless parameters are presented in Figure 14(b). A good collapse of the results for different reduced velocities is obtained even though the work rate is strongly nonlinear. It should be noted that the results would have been slightly different if the tube was not initially centred between its supports. In general, slightly higher contact forces were reported for the case of eccentric tubes (Fisher *et al.* 1991). Fisher *et al.* (1995) showed that the wear work rate and the associated wear volume rate are smaller for the case of eccentric tubes. All of the dimensionless parameters used in this study are summarized in Table 1.

5. SCALING FOR DIFFERENT CONFIGURATIONS

To investigate the applicability of scaling the dimensionless results reported herein, additional configurations with different tube lengths and diameters were analysed (Table 2). These were designated as configurations 2 and 3, respectively. The support stiffness, the damping and the friction are the same as those used in Section 4. Simulations for configurations 2 and 3 were carried out assuming fluid excitation due to a gas flow of density 1·18 kg/m^3. For a reduced velocity of 116·7, the lift response for configuration 1 with a radial clearance of 0·025 mm is 16 times that of configuration 3 with a radial clearance of 0·01 mm.

The response spectra in all three cases are similar in terms of the participating modes. This suggests that the dimensionless parameters described in the previous section can be applied to tubes with different parameter values. Results pertaining to the whole range of clearances obtained from configurations 2 and 3 were computed using the proposed dimensionless parameters and compared with those of configuration 1. Figure 15 shows the contact ratio, the dimensionless r.m.s. impact force, the lift response and the drag response for all configurations. Despite the differences in the clearance range as well as in the tube mass, stiffness and length, the proposed dimensionless parameters yield a remarkable collapse of the responses obtained from the three configurations. The collapse of the results is excellent when comparing the tube response and the impact forces. A

TABLE 2

Parameter values for the three tube configurations

	Configuration		
	1	2	3
Length (mm)	2000	305	617
Diameter (mm)	15	6·35	15·88
Elasticity modulus (GPa)	230	105	106
Wall thickness (mm)	1·5	1·24	0·815
Fundamental frequency (Hz)(support inactive)	3·5	38·6	28·1
Fundamental frequency (Hz)(support active)	15	169·2	122·9
Reduced velocity for 4 m/s	77·8		
Reduced velocity for 6 m/s	116·7	24·5	13·5
Reduced velocity for 8 m/s	155·5		
Maximum modal frequency (Hz)	1281	9781	10420
Time step (ms)	0·1	0·01	0·01

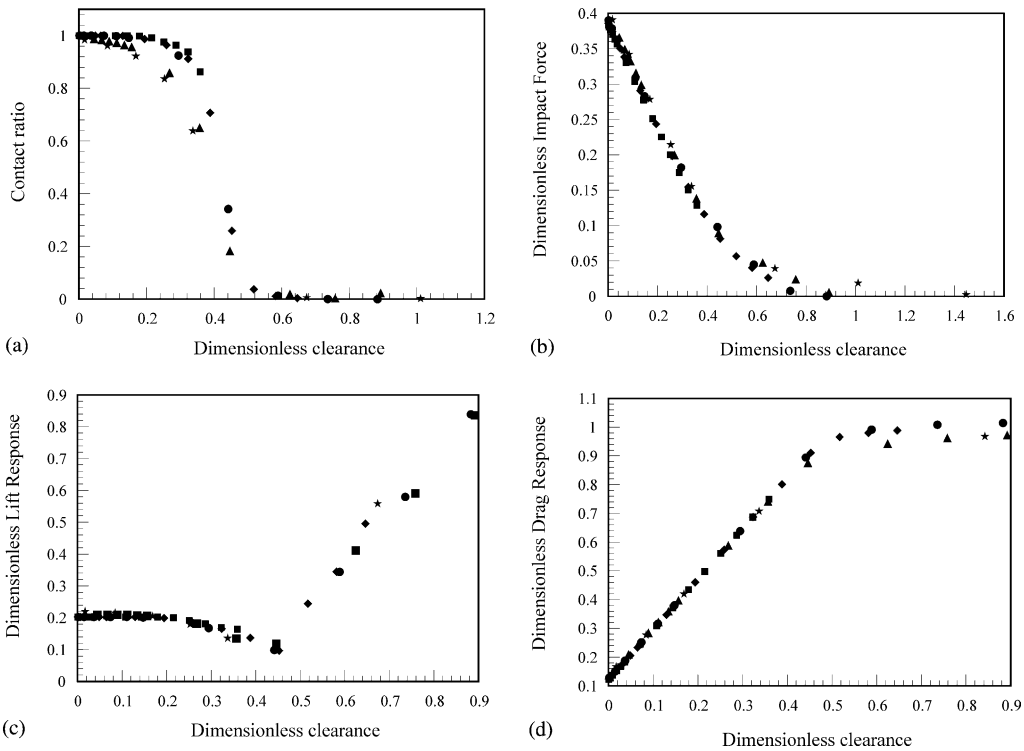

Figure 15. Dimensionless tube response versus. dimensionless clearance for different configurations (no offset): ★, $U_R = 13{\cdot}5$; ▲, $U_R = 24{\cdot}5$; ●, $U_R = 77{\cdot}8$; ◆, $U_R = 116{\cdot}7$; ■, $U_R = 155{\cdot}5$. (a) Contact ratio; (b) r.m.s. impact force; (c) r.m.s. lift response; (d) r.m.s. drag response.

reasonable collapse is also obtained for the contact ratio. However, the contact ratios for configurations 2 and 3 are slightly lower than that of configuration 1 in the early stages of the mode switch. This is attributed to the fact that the ratio of the tube stiffness to the support stiffness is higher for configurations 2 and 3. However, the general behaviour of

the response did not change and the agreement between the various configurations is reasonable given the strong nonlinearity of the phenomenon.

The effectiveness of the loose supports is of great importance. As indicated by Chen *et al.* (1985), support-active conditions prevail when the support clearance is small. In addition, high excitation will also enforce the support-active conditions. Typical values of the diametral support clearance used in heat exchangers are in the range of 0·25 to 0·5 mm (Boucher & Taylor 1996). In this study, it was found that the effectiveness of the support may be entirely determined by the dimensionless support clearance. Support–active mode response takes place when the dimensionless radial clearance is in the range of 0–0·4 regardless of the tube properties and excitation level.

It is important to note that only turbulence excitation is considered in the present study. Thus, when the support becomes inactive, the impact forces and wear rate reduce to zero. However, these effects are also associated with the appearance of lower frequency support-inactive modes. In the presence of fluid-elastic forces, these lower modes may be excited into instability which would rapidly increase vibration amplitude, impacting, and wear rate as so-called "amplitude-limited fluid-elastic instability" develops. This phenomenon is not considered in the present study.

6. EFFECT OF THE SUPPORT OFFSET

Support offset, e, is defined as the axial distance between the centre-line of two successive pairs of flat bars [Figure 7(b)]. In this section, numerical simulations are performed utilizing the tube designated as configuration 3 in the previous section. The tube is considered to be loosely supported by a lattice-bar support having a support offset of 10% of the tube length. For this support offset value, 16 radial clearance values were investigated. The crossflow is assumed to be at a 0° angle with the support axis as shown in Figure 6(b). As mentioned earlier, the lattice support [Figure 7(b)] consists of two pairs of flat bars which form a diamond–shaped support space. Pair B was set at the tip of the tube, while pair A was placed further down the span to produce the desired offset. Details of the tube–support interaction at each of the support pairs were considered.

The contact between the tube and a specific pair depends on the location of this pair on the span. The contact ratio for both pairs is therefore the same when the support offset is zero. As the support offset is introduced, the tube maintains an unequal contact ratio with both pairs. Figure 16(a) depicts the contact ratio between the tube and support pairs A and B. For small dimensionless clearances in the range of 0–0·3, the contact ratio is higher in the case of the support offset, as the offset effectively increases the length of the support. As mentioned earlier, if the clearance is increased, the support begins to lose its effectiveness, a mode switch occurs and the contact ratio drops abruptly. Interestingly, the introduction of a support offset does not change the general behaviour of the contact ratio as a function of the dimensionless clearance. However, Figure 16(a) shows that support offset extends the range of clearance over which the contact ratio remains near unity, thereby reducing the range of clearance over which the mode switch occurs.

The behaviour of contact ratio between the tube and pair B is similar to that of the tube with pair A. The contact ratio for pair B is a little higher than that of pair A in the mode switch region of dimensionless clearance. This is because the support pair B is located at the tip of the tube.

The impact forces created at support pairs A and B are shown in Figure 16(b). The general behaviour of the dimensionless impact force is similar in both cases. In the range of dimensionless clearances up to about 0·1, the introduction of the support offset yields a

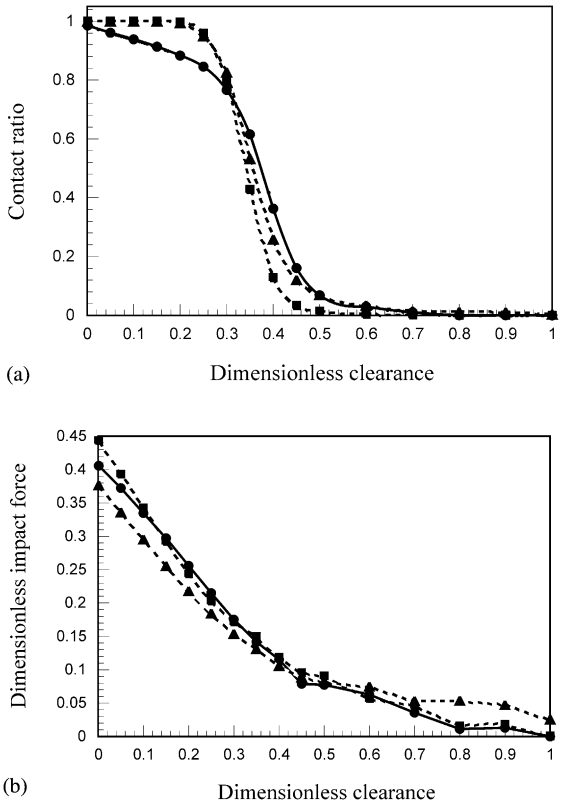

Figure 16. Effect of the support offset on the (a) contact ratio and (b) impact force: ●, 0% offset (pair A and B); ■, 10% offset (pair A); ▲, 10% offset (pair B).

higher r.m.s. impact force at pair A than that for the case of zero offset. On the other hand, a smaller impact force at pair B is obtained up to the clearance at which mode switch occurs (0·45).

The behaviour of a tube with a support offset is very complex. The tube response at a particular clearance and offset is composed of a combination of modes. These modes correspond to the possible linear subsystems, i.e., the unconstrained system, the fully constrained system, the system with support active only at pair A or the system with support active only at pair B. The term support-active at pair B means that the tube is hinged at pair B and can respond in the plane containing the flat bars of pair A as shown in Figure 17(a). Ultimately, the tube can respond in the plane of support B as shown Figure 17(b). Since these planes are not orthogonal for the case of the triangular tube array, mode coupling will generally occur through support contact.

The tube response spectra for supports with a 10% offset are shown in Figure 18. The spectra for a small dimensionless clearance of 0·001 is shown in Figure 18(a) which contains a number of peaks belonging to two different support-active modes. The peaks at frequencies of 120 and 150 Hz correspond to the fundamental frequency of the supports active at B and A respectively. The amplitude of the 150 Hz peak is larger than that of the 120 Hz peak. As the clearance is increased, the amplitude of the 120 Hz peak increases relative to that of the 150 Hz [Figure 18(b)]. At a larger clearance (0·35), a single peak at a frequency of 127 Hz dominates the spectrum [Figure 18(c)]. For a still larger dimensionless clearance (0·4), the band width of the response spectrum increases [Figure 18(d)]. At this

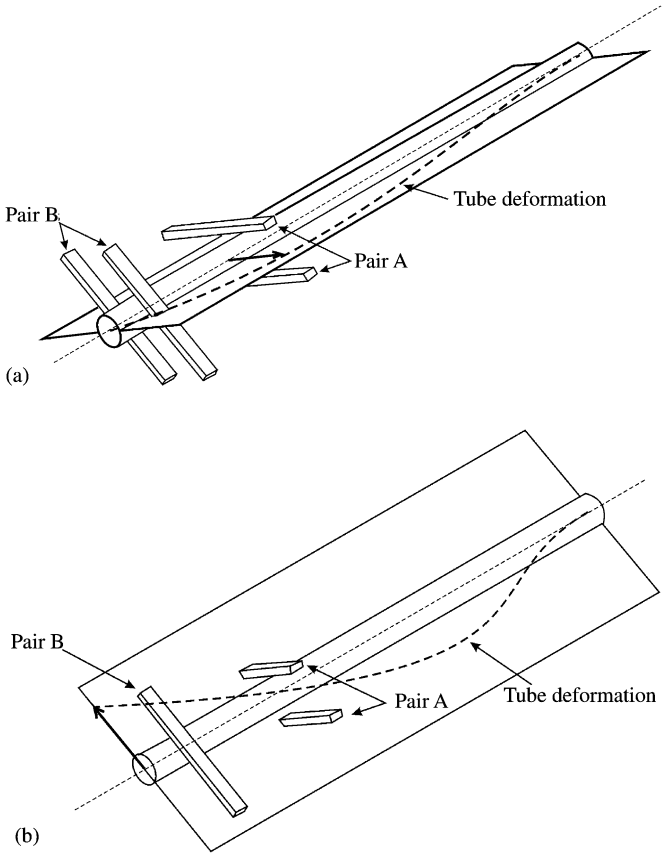

Figure 17. Support-active modes in case of support offset: (a) the system with support active at pair B (tube motion in the plane parallel to pair A); (b) the system with support active at pair A (tube motion in the plane parallel to pair B).

point, the system is in the range of the mode switch which is marked by a flattening of the peaks and the appearance of the lower frequency response [Figure 18(e)]. Moreover, the response spreads over a wider range of frequencies around the first mode. For very large clearances [Figure 18(f)], the spectrum shows the frequencies corresponding to the natural frequencies of the fixed–free configuration.

The predicted dimensionless normal work rates are presented in Figure 19. The introduction of the offset has a dramatic effect on the normal work rate at pairs A and B. For a given dimensionless support clearance in the range of 0 to about 0·3, the normal work rate at pair A is higher than that of pair B. This is attributed to the amount of sliding motion permitted in the plane of pair A. When the offset is zero, the tube sliding motion on pair A meets two types of resistance: (a) the friction opposing the tube motion in both directions, and (b) the flat bars belonging to pair B. As the offset is introduced, the second constraint becomes less effective since it restrains the tube at a point away from the plane containing pair A. Referring to Figure 17(a), pair B creates a vibration node at the tip of the tube. In the plane of pair B, friction is the only resistance to the sliding motion along this pair. This situation is applicable as long as the clearance is small enough to ensure a support active node at the tube tip (pair B). The tube vibration is mainly in the first constrained mode with a frequency of approximately 120 Hz. Therefore, the sliding

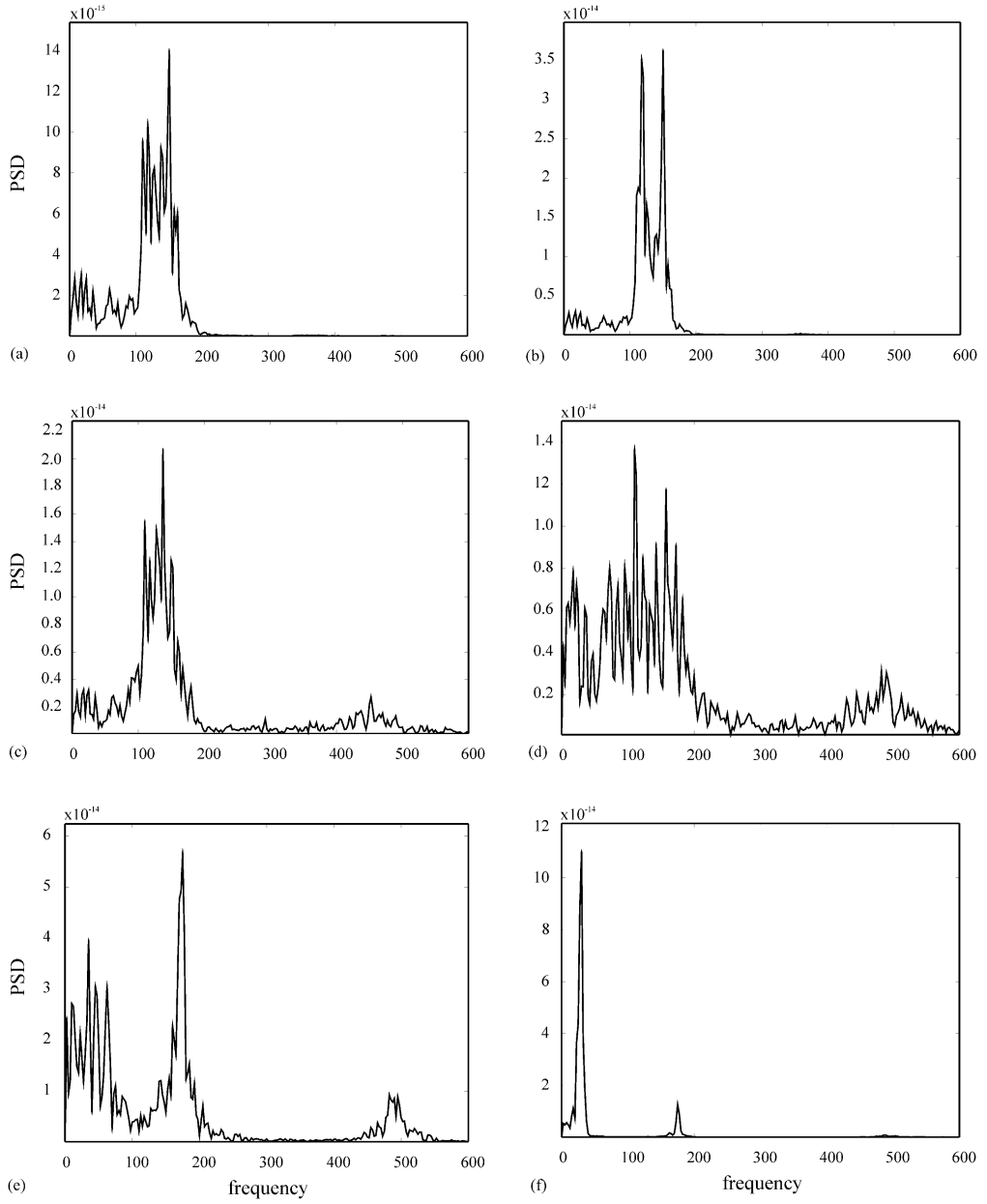

Figure 18. Response spectra of the tube with lattice-bar support (10% offset) and varying dimensionless clearance: (a) 0·001; (b) 0·15; (c) 0·35; (d) 0·4; (e) 0·45; (f) 0·7.

velocity, which is directly related to the frequency of oscillation, is dependent on the location of the support on the tube. Hence, a higher velocity component in this plane is obtained for the case of offset. Moreover, the sliding velocity also depends on the degree of participation of this mode in the overall system response. Now, as the clearance increases, the effectiveness at pair A is reduced. This corresponds to a slight decrease in the vibration frequency for a range of dimensionless clearances up to 0·3. In addition, the r.m.s. impact

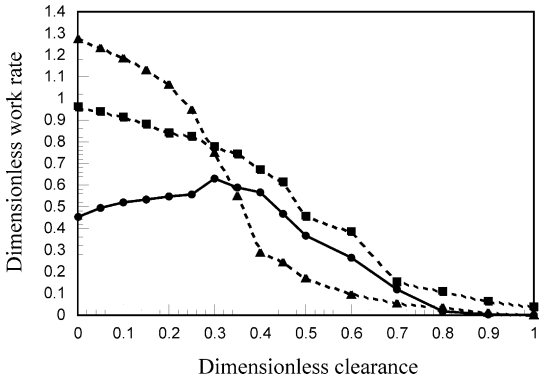

Figure 19. Effect of the support offset on the normal work rate: ●, 0% offset (pair A and B); ■, 10% offset (pair B); ▲, 10% offset (pair A).

force decreases almost linearly as the dimensionless clearance increases. Therefore, the normal work rate, which is the average product of the impact force and the sliding velocity, decreases almost linearly for this range of dimensionless clearance. The frequency decreases dramatically approaching the dimensionless clearance at which the mode switch occurs. This reflects on the work rate, which decreases sharply as it approaches the mode switch. Moreover, the reduction of the r.m.s. impact force contributes to the reduction in the normal work rate. At pair B, energy dissipated through friction is due to the sliding of the tube along the plane containing pair B. This is shown in Figure 17(b), in which the tube displacement in the plane of pair B is presented. Friction resists tube motion in the plane containing pair B. Pair A will create a nodal point at its location as long as the clearance is small. As discussed previously, introducing the offset reduces the physical restraint of the flat bar belonging to pair A to the sliding motion along the flat bars of pair B. This results in a normal work rate higher than the zero-offset support case.

7. MULTI SPAN TUBE CASE

7.1. Finite Element Model

Figure 20 shows the finite element model for a tube supported by three loose supports. The tube was modelled using 30 12 dof elements. Turbulence excitation is modelled as a distributed load along the lower span only with details as described in Section 4.2. The tube was assumed to be clamped into a tube sheet at the lower end. The overall tube length is 3·4 m with an inside and an outside diameter of 13·3 and 15·88 mm, respectively. The three loose supports are placed such that equal spans are maintained and the clearance is assumed to be the same at all supports. The support geometry and flow direction are shown in Figure 6(b) with no lattice-bar offset.

7.2. Results and Discussion

7.2.1. Contact Ratio

Figure 21(a) depicts the contact ratio between the tube and its supports as a function of dimensionless clearance. The support clearance at each support may be normalized by the

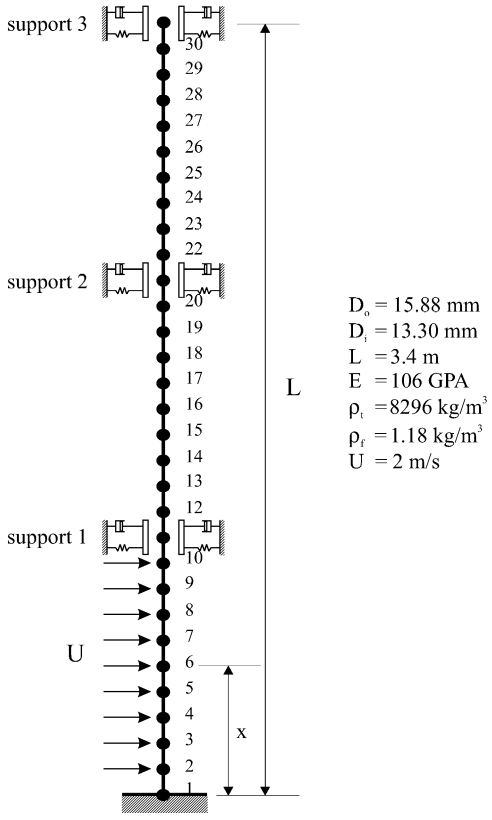

Figure 20. Multi-span tube model.

r.m.s. response at that support. However, in order to compare the tube/support interaction parameters for all supports, support clearances are normalized by a reference tube response value. In this work, the dimensionless clearance is obtained by dividing the clearance by the resultant r.m.s. tube response at support 3 with all supports inactive. The use of the r.m.s. tube response at one of the other supports for normalizing the results would change the curve scales but not the shape of the curves.

The contact ratio behaviour between the tube and support 1 is similar to that of a single-span tube in which the contact ratio initially decreases at a small rate. This is followed by a sharp decrease as the mode switch occurs and the contact ratio approaches zero asymptotically. The contact ratio between the tube and the second support shows quite different behaviour. At a zero clearance, the tube maintains contact with all supports. Since the excitation forces are distributed along the first span only, the deflection in the other spans is not large enough to maintain continuous contact between the tube and either the second or the third support with a nonzero clearance. Thus, as the clearance increases slightly, the contact ratio at the second and third supports decreases dramatically. A further increase in the dimensionless clearance permits intermittent contacts, which excite higher modes. Moreover, the first support becomes less active in resisting the tube motion and a larger tube deflection is then transferred to the second span. Consequently, the deflection of the tube in the neighbourhood of the second support increases significantly as the support clearance increases, leading to an increase in the contact ratio here. This process, in which the contact ratio at the first support decreases

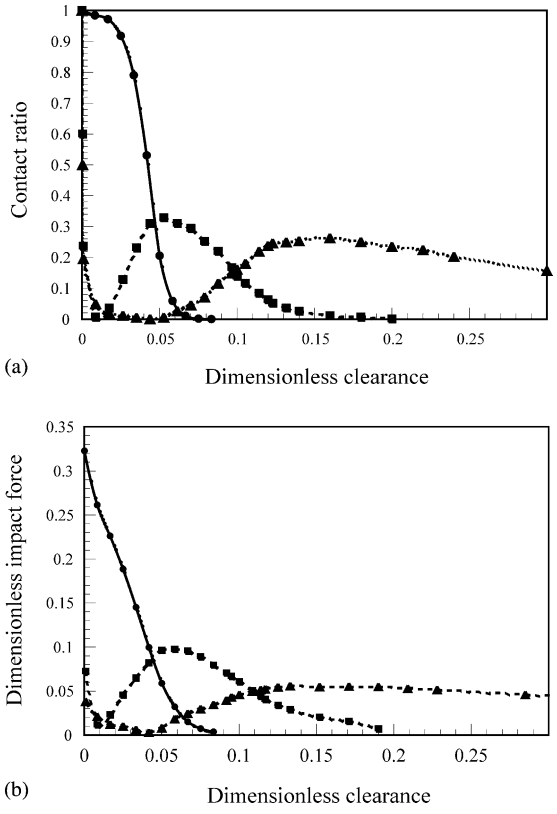

Figure 21. The effect of the clearance on the (a) contact ratio for all supports and (b) r.m.s. impact force for all supports: ●, support 1; ■, support 2; ▲, support 3.

while it increases at the second support (support duty exchange between the first and second supports), continues up to a dimensionless clearance of about 0·05, beyond which a similar duty exchange occurs between supports 2 and 3.

7.2.2. R.m.s. impact forces

The r.m.s. impact forces for the three supports are shown in Figure 21(b) and the behaviour closely mimics that of the contact ratio. The intensity of the impact forces at each of these supports depends strongly on the clearance at these supports as well as the location of the excitation. A process of load redistribution among the three supports takes place as the clearances increase and the effective modal contribution shifts accordingly.

7.2.3. Tube displacement

The dimensionless tube response at $x/L = 0{\cdot}16$ (approximately the middle of the lowest span) in the lift direction is plotted against the dimensionless clearance in Figure 22(a). Generally, increasing the support clearance results in an increase in the dimensionless tube response. However, it can be seen that there are several undulations in the curve, each of which is associated with one of the mode switches discussed in the next section.

Figure 22(b) shows the dimensionless tube response (d_z/d_{zsi}) in the drag direction as a function of the support clearance. Similar to the single-span tube, the tube drag response increases monotonically as the clearance increases up to the point where no contact occurs. Notice that the drag response curve can be divided approximately into four different

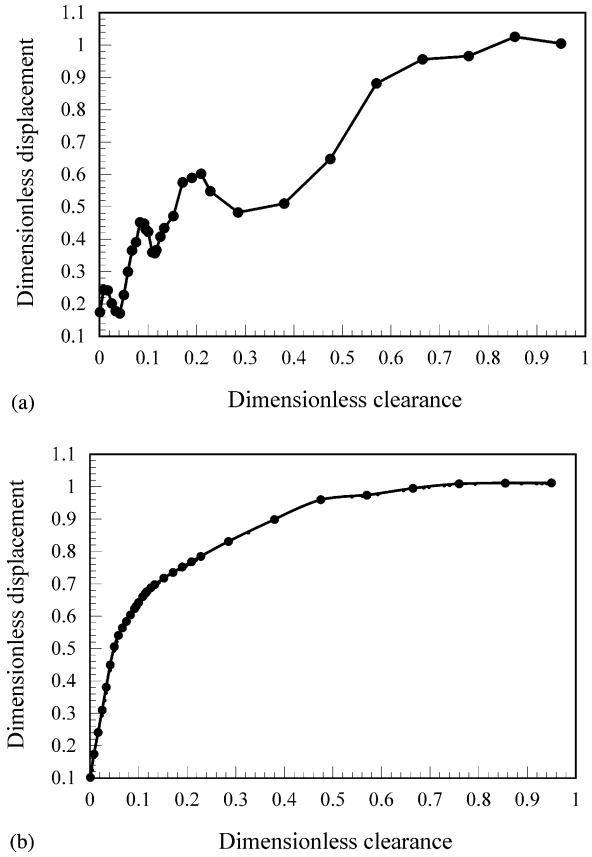

Figure 22. The effect of the clearance on the lower mid-span tube displacement: (a) the lift direction; (b) the drag direction.

regions. Within each of these regions, the dimensionless drag response increases almost linearly as the dimensionless clearance increases. The transition between these regions corresponds to one of the major mode switch events. The fourth region is characterized by a response regime in which the first and second supports are inactive, while the tube maintains little contact with the third support.

7.2.4. Response spectra

The response spectra of the tube lift response (calculated at the first unconstrained node away from the fixed end) for various dimensionless clearances are illustrated in Figure 23. The response spectra of a multi-span tube are very complex because they consist of peaks belonging to combinations of different modes, the appearance of which depends on the effectiveness of each of the three supports. At low dimensionless clearances ($0 < C_r/d_{rsi} < 0{\cdot}05$), the tube maintains a high contact ratio with the first support. This is manifested by the appearance of the high frequency modes in the response spectra. The frequency of the fundamental mode is 30 Hz. However, the dominant mode is 44 Hz (Figure 23(a)). These frequencies correspond to the case in which the tube is effectively restrained at the first support, partially supported at the second, and has little restraint at the third. Within this dimensionless clearance range, the amplitude of the fundamental frequency (30 Hz) increases as the dimensionless clearance increases. This causes the

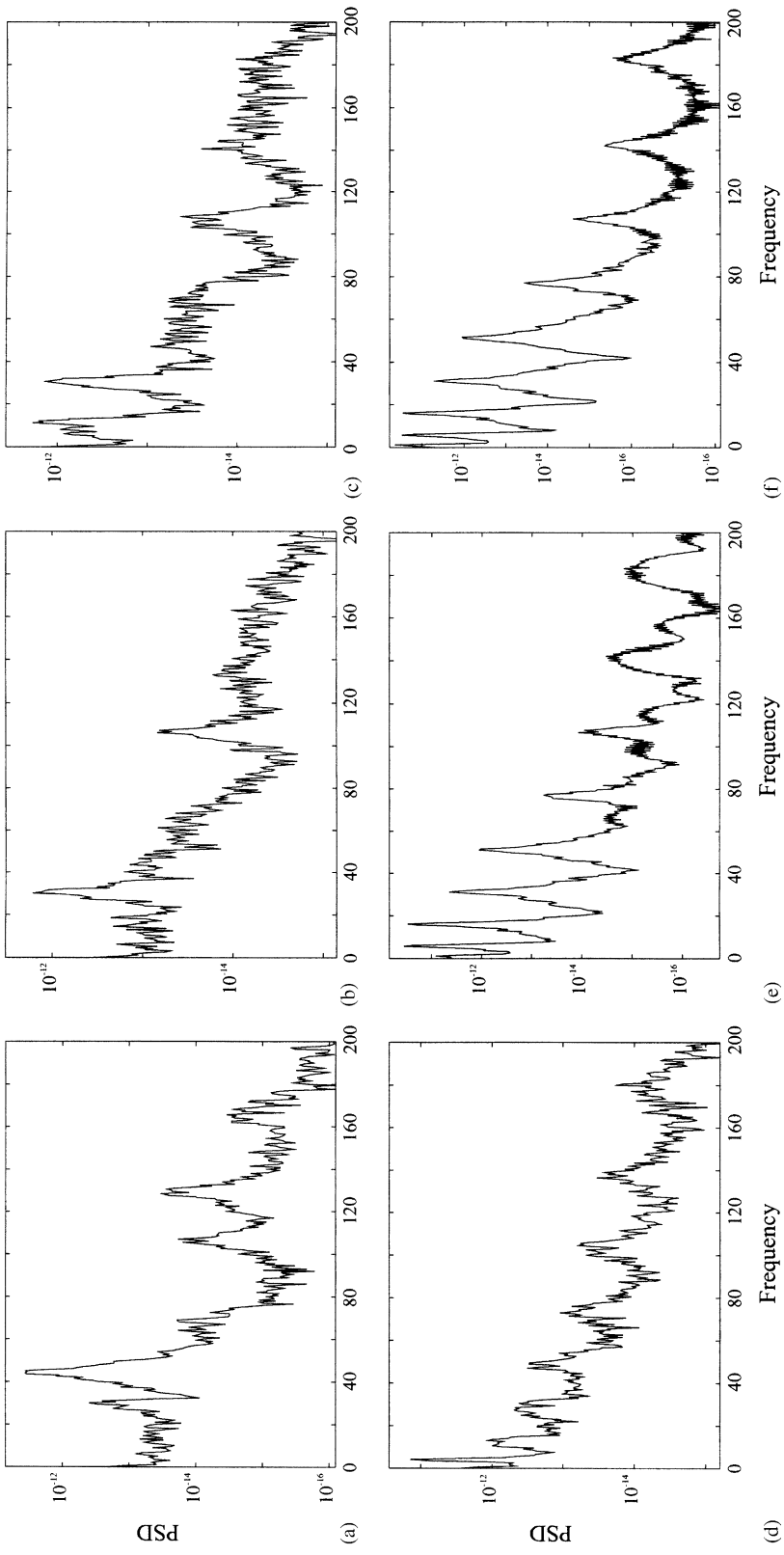

Figure 23. Lift response spectra for various dimensionless clearances: (a) 0·02; (b) 0·05; (c) 0·07; (d) 0·18; (e) 0·8; (f) 0·9.

appearance of the first peak in the lift displacement curve (Figure 22(a)). Finally, the 30 Hz frequency mode becomes the dominant mode at a dimensionless clearance of 0·05 (Figure 23(b)). This corresponds to the configuration in which the tube is fully restrained at the second support, partially restrained at the first support, and has very little restraint at the third support. Moreover, at this dimensionless clearance, the peak of the contact ratio between the tube and the second support occurs (Figure 21(a)). As the dimensionless clearance increases further, the tube faces less restraint at the second support and an increasing restraint at the third support. This is demonstrated by the appearance of a peak at a frequency of 120 Hz. With an increase in the dimensionless clearance, this peak (12 Hz) increases until it becomes dominant at a dimensionless clearance of 0·07 [Figure 23(c)]. This corresponds to the second peak in the lift response curve [Figure 22(a)] and, as can be seen in Figure 21(a), the tube has completely lost contact with the first support. As the dimensionless clearance is further increased, the fundamental frequency is gradually reduced until it reaches 4·0 Hz at 0·18 [Figure 23(d)]. At this dimensionless clearance, the tube has its maximum contact ratio with the third support, while it faces less restraint at the second support. The response spectrum exhibits peaks at the frequencies 31, 51, 76, 107, 141 and 179 Hz, which are approximately the unconstrained tube natural frequencies. On the other hand, the first two peaks are at frequencies around 3·7 and 12 Hz. The domination of these low frequency modes marks the third peak in the lift response curve

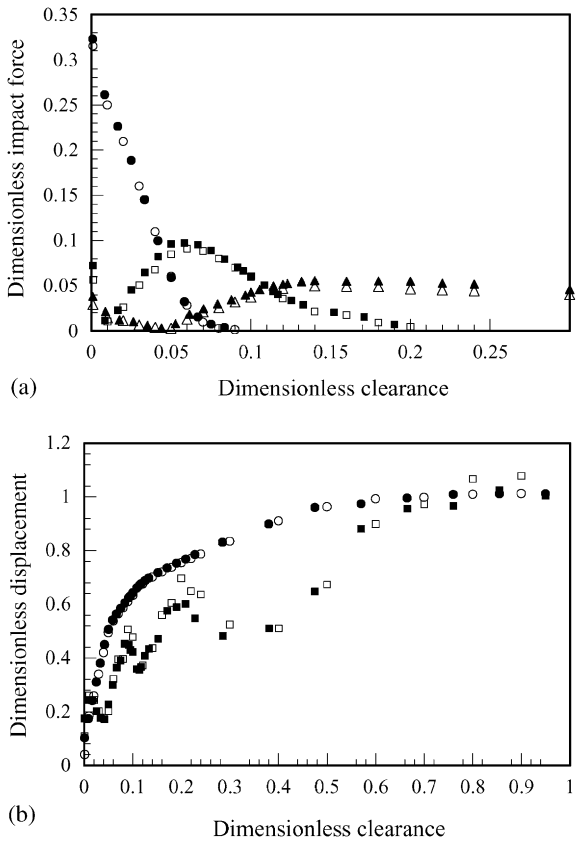

Figure 24. Dimensionless tube response for two flow velocities; open symbols ($U_R = 139{\cdot}7$), closed symbols ($U_R = 279{\cdot}4$): (a) r.m.s. impact force: ●, ○, support 1; ■, □, support 2; ▲, △, support 3; (b) tube displacement in the lift and drag directions: ●, ○, drag displacement; ■, □, lift displacement.

(Figure 22(a)). The second peak frequency (12·0 Hz) progressively increases until it reaches that of the third unrestrained mode (16 Hz). Concurrently, the frequency of the fundamental mode is continuously decreasing [Figure 23(e)]. The mode switch is totally achieved by the appearance of the second unconstrained mode at a dimensionless clearance of 0·5 [Figure 23(f)].

To examine the applicability of the proposed dimensionless parameters to this three span case, additional simulations were performed at a reduced velocity of 279. The results obtained from the two reduced velocities are compared in Figures 24(a) and 24(b). The results show a good collapse of the data for both the impact force at the supports [Figure 24(a)] and for the mid-span r.m.s. displacement in the lower span [Figure 24(b)].

8. CONCLUSION

A tube/support interaction model was implemented in the computer code INDAP to examine the dynamic behaviour characteristics of a tube in the presence of the nonlinear constraints provided by loose lattice-bar supports. Force and displacement time histories obtained from INDAP simulations were found to be in good quantitative agreement with three examples available in the literature.

The effect of the clearance between the tube and the lattice-bar supports on the contact ratio, impact force, lift and drag response, and work rate was investigated. The study involved numerical computations of tube response due to turbulence excitation. The tube behaviour exhibits two distinct dynamic regimes (support-active and support-inactive modes) depending on the clearance and the excitation level. These results are similar to those reported in the literature for other types of tube supports. It is found that, for a fixed level of excitation and centred tubes, increasing the support clearance decreases the r.m.s. impact forces and the contact ratio. This is simply because fewer tube/support contacts are made and their duration is shorter. On the other hand, the lift response of the tube decreases for a range of clearances, then increases, producing a point of minimum response at a certain clearance. This point of minimum response marks the transition in the tube dynamics from the constrained to the unconstrained configuration. This transition in the tube dynamics is also manifested by a change in the drag response from increasing linearly, to levelling off and approaching the r.m.s. tube response of the unconstrained configuration.

The effect of the offset of the lattice-bar supports was also investigated. The results show that offset affects the tube dynamics substantially. In particular, the sliding contact and the impact forces are increased such that the normal work rate is increased. Thus, despite increasing the complexity of the tube response through strong nonlinear coupling at the supports, substantial lattice-bar offset may generate increased wear at the supports.

Simulations of a multi-span tube indicate that, depending on the clearance, the effectiveness of some of the supports is changed. It is observed that a process of load-carrying redistribution takes place among the three supports. Complex response spectra were observed in which multiple mode switches exist as the clearances are increased.

For the first time, the tube response and the associated tube/support interaction parameters have been presented in dimensionless form. Dimensionless parameters effectively collapse the data obtained for the nonlinear response of loosely supported heat exchanger tubes subjected to random turbulence excitation. The applicability of the methodology was confirmed by means of numerical simulations of three different tube configurations. The introduction of these dimensionless scaling parameters expands the power and the utility of the numerical model to predict a wider range of configurations

and flow conditions. This is significant, since the procedure can be applied for design purposes in order to reduce the risk of fretting wear-related failure by controlling the most dominant factor, the dimensionless clearance. These dimensionless parameters also assist in providing physical insights into the complex nonlinear dynamics of the tube in loose supports.

ACKNOWLEDGEMENTS

The authors gratefully acknowledge the financial support of the Natural Science and Engineering Research Council of Canada (NSERC).

REFERENCES

ANTUNES, J., AXISA, F., BEAUFILS, B. & GUILBAUD, D. 1990a Coloumb friction modelling in numerical simulations of vibration and wear work rate of multispan tube bundles. *Journal of Fluids and Structures* **4,** 287–304.

ANTUNES, J., AXISA, F. & VENTO, M. 1990b Experiments on vibro-impact dynamics under fluidelastic instability. In *Flow-Induced Vibration 1990* (ed. S.S. Chen), PVP-Vol. 189, pp. 127–138. New York: ASME.

AXISA, F., ANTUNES, J. & VILLARD, B. 1988 Overview of numerical methods for predicting flow-induced vibration. *ASME Journal of Pressure Vessel Technology* **110,** 6–14.

BLEVINS, R. D. 1979 Flow-induced vibrations in nuclear reactors: a review. *Progress in Nuclear Energy* **4,** 24–49.

BOUCHER, K. & TAYLOR, C. 1996 Tube support effectiveness and wear damage assessment in the U–bend region of nuclear steam generators. In: *Flow-Induced Vibrations1996* (ed. M. Pettigrew), PVP-Vol. 328, pp. 285–296. New York: ASME.

CHEN, S. S, JENDRZJCZYK, J.A. & WAMBSGANSS, M. W. 1985 Dynamics of tubes in fluid with tube-baffle interaction. *ASME Journal of Pressure Vessel Technology* **107,** 7–17.

DAVIS, H. & ROGERS, R. 1979 The vibration of structures elastically constrained at discrete points. *Journal of Sound and Vibration* **63,** 437–447.

DOKAINISH, M. 1988 *Incremental Nonlinear Dynamic Analysis Program: Verification Manual*. McMaster University, Canada.

DOKAINISH, M. & SUBBARAJ, K. 1989 A survey of direct time-integration methods in computational structural dynamics—I explicit methods. *Computers & Structures* **32,** 1371–1386.

FISHER, N., CHOW, A. & WECKWERTH, M. 1995 Experimental fretting-wear studies of steam generator materials. *ASME Journal of Pressure Vessel Technology* **117,** 312–319.

FISHER, N., OLESEN, M., ROGERS, R. & KO, P. 1989 Simulation of tube-to-support dynamic interaction in heat exchange equipment. *ASME Journal of Pressure Vessel Technology* **111,** 378–384.

FISHER, N., PETTIGREW, M. & ROGERS, R. 1991 Fretting wear damage prediction in the inlet region of nuclear steam generators. In *Institution of Mechanical Engineers, International Conference on Flow Induced Vibrations,* IMechE 1991-6, Brighton, U.K., pp.149–158, London: IMECHE.

FRICKER, A. 1992 Numerical analysis of the fluidelastic vibration of a steam generator tube with loose supports. *Journal of Fluids and Structures* **6,** 85–107.

HASLINGER, K., MARTIN, M. & STEININGER, D. 1987 Pressurized water reactor steam generator tube wear prediction utilizing experimental techniques. In *Proceedings BHRA Conference on Flow-Induced Vibrations*, Bowness-on-Windermere, U.K. (ed. R. King), K2, pp. 437–448. Cranfield: BHRA.

HASLINGER, K. & STEININGER, D. 1995 Experimental characterization of sliding and impacting friction coefficients between steam generator tubes and AVB supports. *Journal of Sound and Vibration* **181,** 851–871.

HUNT, K. H. & CROSSLEY, F. R. 1975 Coefficient of restitution interpreted as damping in vibroimpact. *Journal of Applied Mechanics* **43,** 440–445.

OENGÖREN A. & ZIADA, S. 1995 Vortex shedding, acoustic resonance and turbulent buffeting in normal triangle tube arrays. In *Flow-Induced Vibrations* (ed. P. Bearman), pp. 295–313. Rotterdam: A. A. Balkema.

Païdoussis, M. P. 1982 A review of flow-induced vibrations in reactors and reactor components. *Nuclear Engineering and Design* **74,** 31–60.

Pettigrew, M. 1981 Flow-induced vibration phenomenon in nuclear power station components. *Power Industry Research* **1,** 97–133.

Rao, M., Gupta, G., Eisinger, F., Hibbitt, H. & Steininger, D. 1987 Computer modeling of vibration and wear multispan tubes with clearances at tube supports. In *Proceedings BHRA Conference on Flow-Induced Vibrations*, Bowness-on-Windermere, U.K. (ed. R. King), K3, pp. 449–465. Cranfield: BHRA.

Rao, M., Laskowski, L., Srikantiah, F. & Ahluwalia, H. 1997 Prediction of tube wear to flow-induced vibration in PWR steam generators. In *4th International Symposium on Fluid–Structure Interactions, Aeroelasticity, Flow-Induced Vibration and Noise,* Dallas (eds M. Païdoussis, M. K. Au-Yang, W. J. Bryan, S. S. Chen, Y. A. Hassan, F. J. Moody, S. J. Price, D. S. Weaker, S. Ziada.), Vol. 2, pp. 257–264. New York: ASME.

Rogers, R. & Pick, R. 1977 Factors associated with support plate forces due to heat exchanger tube vibratory contact. *Nuclear Engineering and Design* **44,** 247–253.

Sauvé, R. 1996 A computational time domain approach to fluidelastic instability for nonlinear tube dynamics. In *Flow-Induced Vibrations1996*, (ed. M. Pettigrew), PVP-Vol. 328, pp. 327–335. New York: ASME.

Sauvé, R. & Teper, W. 1987 Impact simulation of process equipment tubes and support plates-a numerical algorithm. *ASME Journal of Pressure Vessel Technology* **109,** 70–79.

Tan, X. & Rogers, R. 1996 Dynamic friction modelling in heat exchanger tube simulations. In *Flow-Induced Vibrations1996* (ed. M. Pettigrew), PVP-Vol. 328, pp. 347–358. New York: ASME.

Taylor, C., Boucher, K. & Yetisir, M. 1995 Vibration and Impact forces due to two-phase cross-flow in U-bend region of nuclear steam generators. In *Flow-Induced Vibrations* (ed. P. Bearman), pp. 401–412. Rotterdam: Balkema.

Weaver, D. S. & Fitzpatrick, J. 1988 A review of cross-flow induced vibrations in heat exchanger tube arrays. *Journal of Fluids and Structures* **2,** 73–93.

Weaver, D. S. & Schneider, W. 1983 The effect of flat bar supports on the crossflow induced response of heat exchanger U-tubes. *ASME Journal of Pressure Vessel Technology* **105**, 775–781.

Yetisir, M. 1985 The vibro-impact of heat exchanger U-bend tubes with flat bar supports. M. Eng. thesis, McMaster University, Canada.

Yetisir, M., Mckerrow, E. & Pettigrew, M. 1997 Fretting wear damage of heat exchanger tubes: a proposed damage criterion based on tube vibration response. In *4th International Symposium on Fluid-Structure Interactions, Aeroelasticity, Flow–Induced Vibration and Noise,* Dallas (eds M. Païdoussis, M. K. Au-Yang, W. J. Bryan, S. S. Chen, Y. A. Hassan, F. J. Moody, S. J. Price, D. S. Weaker, S. Ziada.), Vol. 2, pp. 291–299, New York: ASME.

Yetisir, M. & Weaver, D. 1986 The dynamics of heat exchanger U–bend tubes with flat–bar supports. *ASME Journal of Pressure Vessel Technology* **108,** 406–412.